

# Stationary atmospheric responses to an idealized sea surface temperature anomaly in the Southern Ocean

GUILLAUME MAZE \*

*Laboratoire de Physique des Océans, UMR 6523, Ifremer, CNRS, IRD, UBO, Plouzané, France*

FABIO D'ANDREA

*Laboratoire de Météorologie Dynamique, Ecole Normale Supérieure, Paris, France*

ALAIN COLIN DE VERDIÈRE

PATRICE KLEIN

*Laboratoire de Physique des Océans, Brest, France*

## ABSTRACT

The stationary atmospheric response to an idealized sea surface temperature anomaly (SSTa) is studied with a quasi-geostrophic atmospheric model of the Southern Hemisphere. Sensitivity of the stationary response to mid-latitude SSTa location is determined and responses decomposed on vertical modes.

The SSTa almost directly forces baroclinic responses, inducing warm air anomalies 40 to 50 degrees downstream, eastward, to the SSTa. These baroclinic responses arise from an equilibrium between the SSTa-induced anomalous vortex stretching and (i) advection by the quasi-stationary flow and (ii) dissipation by high frequency eddies.

The barotropic response consists of a midlatitude ridge (trough) and a South Pole trough (ridge) for SSTa localized from the Drake Passage to the Western Indian ocean (from South of Australia to the center of the Pacific ocean). This response can be further decomposed into (i) a zonally asymmetric component – a quasi-stationary wave train forced by a barotropic ridge downstream of the SSTa and (ii) a zonal mean component similar to a meridional shift of westerlies and hence a Southern Annular Mode (SAM) like pattern. The former component is phase locked with the SSTa position while the latter has a phase which depends on the relative SSTa position with regard to the background quasi-stationary wave pattern. We show that the barotropic downstream ridge response is responsible for modifying the low frequency eddy-mean flow interactions through relative vorticity fluxes and inducing the bipolar projection of the zonal mean response.

Accepted for publication in *Journal of Climate*, 2011, March 18th  
Contact: gmaze@ifremer.fr

## 1. Introduction

The Southern Hemisphere mid-latitudes are characterized by strong zonal jets in the atmosphere and a strong zonal current in the ocean, the ACC (Antarctic Circumpolar Current). The principal mode of atmospheric variability is the hemispheric seesaw described under different names such as "zonal wind vacillation" and "high latitude mode" (Kidson 1988; Hartmann and Lo 1998). Following Thompson and Wallace (2000), we will refer to this mode as the southern annular mode or SAM. The SAM has been shown to dominate the large scale Southern Hemisphere coupled variability (Hall and Visbeck 2002; Simmonds 2003; Codron 2007).

Other studies (e.g. White 2004, and references therein) tend to attribute more importance to a coupled mode of

variability called Antarctic Circumpolar Wave. This mode would explain the fact that sea surface temperatures (SST) anomalies were observed to propagate eastward along the ACC from the mid 80s to mid 90s (Connolley 2002). Works by (Maze et al. 2006, hereafter M06) and Verdy et al. (2006) show how the eastward propagation can be largely explained as a passive transport of SST anomalies by the ACC, where the SST anomalies are generated by the SAM through Ekman surface heat flux or through remote forcing by the El-Niño Southern Oscillation (ENSO). An oceanic feedback on the atmospheric forcing is present though weak and is likely to increase the lifespan of SST anomalies (M06, Watterson 2000, 2001). The importance of this feedback depends crucially on the atmospheric response to the SST anomaly.

During the second half of the twentieth century, positive trends in geopotential height anomalies over the pole and at mid-latitudes were observed (Thompson and Solomon 2002). These trends project positively on the SAM pattern (Thompson and Wallace 1998). An extensive literature has been produced to explain this trend and two causes of anthropogenic origin are clearly identified (i) ozone depletion in the polar stratosphere – reducing shortwave radiation absorption, cooling the polar air and through multiple dynamical responses inducing a positive shift in the SAM – (e.g., Gillett and Thompson 2003; Perlwitz et al. 2008) and (ii) warming in the global tropical oceans (e.g., Grassi et al. 2005). Unlike the ozone depletion mechanism, the role of tropical ocean’s warming on the SAM trend is still being debated among scientists though, simply because the Southern Hemisphere atmospheric response to ocean’s warming can show different and contradictory patterns (see Li et al. 2010, and references therein).

Interactions between sea surface temperatures anomalies (in the tropics and extratropics) and the atmospheric circulation in mid-latitudes have long been studied (e.g., Smagorinsky 1953). But the response of the atmosphere in mid-latitudes is in general small in comparison to its internal variability, which makes it very difficult to measure. Moreover many experiments have been conducted making use of general circulation models both in a coupled or in a forced configuration and large differences in behavior have been found depending on the region, the season and the model used. (See Kushnir et al. (2002) and more recently Li et al. (2010) and references therein). When a dynamical balance is established between eddy forcing and linear advection, the atmospheric response can resemble the large scale modes of unforced atmospheric variability (Peng and Robinson 2001; Son and Lee 2005; Watterson 2010). However, given different large scale basic states, different responses are possible in terms of linear response to heating (Hall et al. 2001). According to the basic state, the nonlinear effect of the transient baroclinic eddy forcing can also become more or less important and characterized by different timescales of action (Peng and Whitaker 1999; Inatsu et al. 2003; Kravtsov et al. 2009).

For all the uncertainties listed above, we propose in this study to determine the atmospheric response to an idealized SST anomaly in the Southern Ocean. The strategy is to focus on the stationary response sensitivity to a mid-latitude SSTa forcing position in order to answer the following questions (i) what is the potential impact of an SSTa transported by the ACC on the overlying atmosphere and (ii) is the SAM sensitive to mid-latitude SSTa? In section 2 the model setup is described in detail, along with a description of the experiments conducted. In section 3 the atmospheric responses are described, and in section 4 their dynamical balance is explained. Results are discussed in section 5 and we conclude in section 6.

## 2. Model and experiments

### a. Model description

The atmospheric model (see figure 1) is quasi-geostrophic (QG) with global domain on the sphere and pressure as a vertical coordinate; it was developed by Marshall and Molteni (1993). A version of this model, coupled to a slab mixed ocean layer, was used by D’Andrea et al. (2005) and M06 for studies of the North Atlantic and the Southern Ocean climate variability. The conservation equation of the quasi-geostrophic potential vorticity (PV):

$$\frac{\partial q}{\partial t} = -J(\psi, q) - \frac{f_0 R}{C_{pa}} \frac{\partial}{\partial p} \left( \frac{Q}{p\sigma} \right) - D(\psi) + S \quad (1)$$

with

$$q = \nabla^2 \psi + f + f_0^2 \frac{\partial}{\partial p} \left( \frac{1}{\sigma} \frac{\partial \psi}{\partial p} \right) \quad (2)$$

is solved on the sphere with a T21 horizontal resolution (triangular truncation) at the pressure levels 200, 500 and 800hPa and integrated in time with a predictor-corrector scheme (first order Adams-Bashforth- Mouton) with a time step of 1 hour. The discretized PV prognostic equations are:

$$\frac{Dq_1}{Dt} = -D_1 + S_1 \quad (3)$$

$$\frac{Dq_2}{Dt} = -D_2 - \frac{Q_{650}(\psi_{2,3}, T)}{K_b R_b^2 C_{pa}} + S_2 \quad (4)$$

$$\frac{Dq_3}{Dt} = -D_3 + \frac{Q_{650}(\psi_{2,3}, T)}{K_b R_b^2 C_{pa}} + S_3 \quad (5)$$

where  $D \cdot / Dt = \partial_t \cdot + J(\psi_i, \cdot)$  is the total derivation operator including PV advection by the QG streamfunctions  $\psi_i$ .  $D_i$  represent linear dissipation terms including Ekman dissipation (orography dependent) and Newtonian thermal relaxation between the layers. Orographic effects are included in the PV definition at the lower level 3 (800hPa).

[Figure 1 about here.]

Recent studies have shown that sea surface temperature fronts can influence the atmosphere up to the tropopause level through vertical penetration of anomalous air-sea fluxes (Minobe et al. 2008). However, given the QG hypothesis, we don’t expect this frontal process to occur in our model. Following previous studies (e.g., Peng and Whitaker 1999; Ferreira and Frankignoul 2005, 2008, and M06), we will assume the penetration of the air-sea surface diabatic forcing to be contained into the lower atmosphere, i.e. to be no higher than 500hPa. In the lower layer the diabatic heat source is computed as  $Q_{650} = (g/\Delta p)F$  where  $g/\Delta p$  ( $\Delta p = 450 \text{ mb}$ ) is a measure of the lower layer thickness and  $F$  represents air-sea turbulent (sensible and latent) heat

fluxes. The second term on the r.h.s. of (4)-(5) is thus the PV tendency due to heat exchanges with the ocean. It depends on  $Q_{650}$  and  $C_{pa}$  the specific heat at constant volume for dry air,  $K_b = f_0 p_b / (R \delta p)$  the coefficient linking streamfunctions at 500hPa and 800hPa to the temperature at 650hPa through the thermal wind balance and  $R_b = 450km$  the Rossby radius of the lower layer (these coefficients appear when the second r.h.s. term of (1) is discretized). The air-sea turbulent heat flux  $F$  is given by the bulk aerodynamic formula:

$$F(\psi_{2,3}, T) = \rho_a C_D C_{pa} (1 + B^{-1}) |\mathbf{U}_s| (SST - T_s) \quad (6)$$

where  $\rho_a$  is the dry air density,  $C_D = 1.3 \times 10^{-3}$  a constant drag coefficient,  $B = 0.5$  the Bowen factor (ratio between sensible and latent heat fluxes),  $|\mathbf{U}_s|$  the surface wind intensity,  $SST$  the sea surface temperature and  $T_s$  the surface atmospheric temperature. Surface atmospheric variables are taken at 10m height.

We introduced in the PV equations a time-independent source term  $S_i$  that represents all adiabatic and subgrid processes (D’Andrea and Vautard 2000) to give the model a realistic wintertime climatology. Winter was chosen as the season where coupling is strongest between the atmosphere and the ocean. The forcing term  $S_i$  is computed empirically as the mean residual of the equation (3-4-5) with respect to observations following the method introduced by Roads (1987). The data used as "observations" were twice daily ECMWF analysis data set ranging from June 1979 to August 1993 (ERA-15, Gibson et al. 1996) for June-July-August, JJA, and SST from Reynolds and Smith (1994). In the case of the Southern Hemisphere this method gave a considerable high pressure error over the Antarctic continent. Consequently, we added a zonal mean temperature correction to all  $S_i$  (see appendix 7 for more details).

Because the atmospheric heat source  $Q_{650}$  is not directly prescribed but depends on the SST through air-sea heat fluxes, see (6): sea surface atmospheric variables need to be diagnosed. The method used is a local linear relation between variables of the atmospheric lower layer and the sea surface. Local wind components are linearly computed from those at 800hPa (diagnosed from  $\psi_3$  obtained by inversion of  $q_3$ ). Local sea surface atmospheric temperature  $T_s$  is linearly computed from the temperature at 650hPa diagnosed using the thermal wind balance between the 500hPa and 800hPa levels. The same data set used to compute forcing terms  $S_i$  (see above) is analyzed to derive local coefficients of these linear relations. Surface wind amplitude is found to be approximately half the wind at 800hPa and surface temperature 1.2 times the one at 650hPa.

## b. Description of the experiments

We carried out 14 experiments, all of them under perpetual JJA conditions, with idealized SST anomalies (SSTa) centered at latitude  $47^\circ S$  and 14 longitudes equally spaced along a latitude circle, starting from the Greenwich’s meridian (see plot A in Fig.2).

As reference for these experiments, a control run is performed with the climatological SST field from a fully coupled version of the model that was studied by M06 (we checked that using this SST field instead of the observation dataset from Reynolds and Smith (1994) used to compute  $S_i$  terms doesn’t induce significant source/sink of PV). The stationary atmospheric response to one of the SST anomalies is defined as the long term mean difference between the simulation with SSTa and the control one.

The idealized SSTa used in the present study has a 2D Gaussian shape. It has been fitted on the mean composite SSTa found by M06 (see their figure 6) and it synthesizes the aspect of a typical SSTa in mid-latitudes of the Southern Ocean. The SST anomaly has a spatial scale of  $80^\circ$  in the zonal direction and  $10^\circ$  in the meridional one, i.e. 6000km by 1200km at mid-latitudes (see plot B in Fig.2).

Many studies force an atmospheric model with SSTa of a few degrees of amplitude in order to enhance the response by increasing the signal/noise ratio (Kushnir et al. 2002). However, a major drawback of this method is that it requires a linear downscaling of the response amplitude to be expressed for a SSTa of  $1^\circ C$  in order to compare results from one study to another. Because of the low numerical cost of the model used in the present study, we can afford to avoid this method. Having fixed the SSTa to a realistic, although still large, amplitude of  $1^\circ C$ , we estimated that integrations length of 50 years were necessary to obtain large statistically significant centers of action in response patterns. This time scale makes our responses eventually valid for climatic trends as those discussed in the introduction. Note, that in order to analyze simple maps without the need to overlay significant pattern regions, the integrations performed were of 200 - perpetual winter - years. We will keep in mind that patterns are statistically robust over most of the domain presented.

The control run climatology has been verified to reproduce key features of the Southern Hemisphere circulation reasonably. For example, the latitude of maximum zonal winds (about  $23 m s^{-1}$ ) is around  $40^\circ S$  at 500hPa, which compares well with observational estimates (see Fig.1 in Hartmann and Lo 1998, for instance). More details about the control simulation climatology can be found in Maze (2006). Here we present two fields relevant to our study. In plots C and D of Fig.2 are shown the barotropic components of the quasi-stationary waves and the SAM – defined as the first EOF of the geopotential height anomalies. At mid-latitudes the quasi-stationary wave pattern shows two

high pressure systems in the Atlantic and Indian regions and two low pressure systems South of Australia and in the Western Pacific regions. They spiral southwestward to over Antarctica. The SAM exhibits a maximum at mid-latitudes southwest of Australia and a minimum in the Indian sector of Antarctica. Both fields are realistic and will be discussed in the following sections.

[Figure 2 about here.]

### 3. Description of stationary atmospheric responses to SSTa

#### a. Responses at pressure levels

SST anomalies induce anomalous air-sea heat fluxes. These in turn force anomalous heat sources in the lower layer of the atmosphere. Air-sea heat flux anomalies have a pattern very similar to the SSTa itself (not shown). The 14 experiments ensemble mean amplitude of  $F$  stationary responses is  $21.0 \text{ W m}^{-2}$ . They varies from  $26.5 \text{ W m}^{-2}$  for experiment with SSTa centered at 51E to  $13.3 \text{ W m}^{-2}$  for experiment with SSTa centered at 180E. These amplitudes correspond to heating rates at 650mb of  $0.4 \text{ K day}^{-1}$ ,  $0.5 \text{ K day}^{-1}$  and  $0.2 \text{ K day}^{-1}$ ; values pretty much in line with standard forcing (recently Butler et al. 2010, used values of  $0.5 \text{ K day}^{-1}$  to study atmospheric responses to climatic change induced heat anomalies). For other atmospheric variables, we also found larger responses amplitude for SSTa centered in the Atlantic/Western Indian sector and smaller responses amplitude for SSTa centered in the Western Pacific.

Analysis of patterns and amplitudes from the 14 experiments has shown that responses may be grouped in two sets, each well represented by results from experiments where SSTa are centered at 0E and 180E shown in Fig.(3)-a-f. These two key experiments among the 14 we conducted will be referred to as SSTa-0E and SSTa-180E hereafter in the study.

Stationary atmospheric responses in geopotential height at 200, 500 and 800hPa and temperature at 650hPa are shown in figure 3, left and right columns for experiments SSTa-0E and SSTa-180E respectively. Note that to plot the geopotential height response we inverted the quasi-geostrophic PV in equation (2) to get the geostrophic streamfunction and then computed the geopotential through:

$$\nabla^2 Z = \frac{1}{g} \nabla f \nabla \psi \quad (7)$$

[Figure 3 about here.]

Fig.(3) shows the geopotential height response in the vicinity of the SSTa (represented in Fig.(3)-a-f) to around 60 degrees eastward being positive in the upper troposphere at 200hPa and 500hPa and negative at the lower

level of 800hPa. In this region close to the SSTa, the response amplitude is quite similar in all experiments: on average about  $-3m$  at 800hPa and  $10/12m$  at 500hPa. Previous numerical studies (Frankignoul 1985; Kushnir et al. 2002) and observations (Rodwell and Folland 2002; Czaja and Frankignoul 2002) had shown a wide range of atmospheric response amplitude: from  $10m.K^{-1}$  to  $40m.K^{-1}$  at 500hPa. Even if our results are clearly in the lower part of this range, one should notice that these amplitudes had all been determined in the Northern Hemisphere and that a direct quantitative comparison needs to be conducted carefully.

Local atmospheric responses, in the vicinity of the SSTa direct forcing, show no fundamental differences among the 14 experiments. This response is baroclinic, a feature clearly seen in the temperature anomaly at 650hPa (Fig.3:e-j). Pressure anomalies positive at 500hPa and negative at 800hPa dilate the lower layer and induce a warm temperature anomaly of  $0.7^\circ C$  eastward of the SSTa. Fig.3:e-j show a very similar pattern between experiments SSTa-0E and SSTa-180E, again representative of all the other 12 locations of SSTa forcing.

The very large scale structure of atmospheric responses are in turn different and discriminate the two sets of experiments introduced earlier in the section. On one hand, the experiment SSTa-0E shows far from the direct SSTa forcing region, geopotential height anomalies positive at mid-latitudes and negative over the South Pole: an equivalent barotropic pattern which thus extends from 200hPa down to 800hPa. On the other hand, experiment SSTa-180E shows geopotential height anomalies of opposite sign compared to the SSTa-0E case, albeit enhanced over the South Pole and weakened at mid-latitudes. These two large scale patterns are relevant for the rest of the experiments. Features from the SSTa-0E case are similar for all other experiments located clockwise from the Drake passage to the western Indian Ocean (experiments denoted as light black circles in Fig. 2-A) whereas the SSTa-180E case is relevant for experiments with SSTa located between South of Australia and the center of the Pacific Ocean (heavy black circles in Fig. 2-A). Outside these broad regions (light black dashed circles in Fig. 2-A) weak responses exhibit intermediate patterns between the two extreme phases of the SSTa-0E and SSTa-180E experiments that we don't discuss here.

#### b. Vertical structure of responses

The visual inspection of all atmospheric responses suggests the superposition of an equivalent-barotropic large scale response onto a local baroclinic one, the former being dependent on the SSTa location while the latter is not. These different behaviors of the atmospheric response with respect to its apparent vertical structure lead us to project responses on vertical modes. This greatly simplifies the

interpretation of the results.

The three pressure levels of the model can be projected onto one barotropic and two baroclinic modes (see appendix 8 for more details). The barotropic mode of the response is proportional to the vertical mean; the first baroclinic mode is related to temperature anomalies having the same sign throughout the depth of the atmospheric column whereas the second baroclinic mode is related to temperature anomalies of opposite signs in the lower and upper layers<sup>1</sup>. Also note that the different Rossby radius of deformation of the upper and lower layers imply that the first (second) baroclinic mode is mainly related to the upper (lower) layer temperature. Figures 4, 5 and 6 show the detailed geopotential height responses of Fig.(3) when projected on the three vertical modes.

[Figure 4 about here.]

1<sup>st</sup> baroclinic mode responses are similar for all 14 experiments in the midlatitude band. Fig.(4)-A-B show negative geopotential height anomaly eastward of the SSTa, of about  $-8m$  and  $-5m$  amplitude. 1<sup>st</sup> baroclinic mode responses are maximum in amplitude for SSTa located from the Atlantic to the East Indian Ocean ( $-14m$  for experiment with SSTa centered at 30W) and minimum for SSTa located in the Western Pacific (about  $-4m$ ). This negative 1<sup>st</sup> baroclinic mode response is the sign of a stationary positive temperature anomaly throughout the depth of the atmospheric column just downstream to the SSTa (see Eq.A5). Note that this warm temperature response is associated, symmetrically to the South Pole, with a cold one (positive geopotential height response) albeit of a smaller amplitude. Over the South Pole however, 1<sup>st</sup> baroclinic mode responses differ among the 14 experiments. Positive (negative) geopotential height anomalies, a cooling (warming) of the atmospheric air column, are found over the South Pole for experiments with SSTa located between the Drake passage and the western Indian Ocean (from South of Australia to the center of the Pacific Ocean).

2<sup>nd</sup> baroclinic mode responses, shown in Fig.(4)-C-D, are restricted to mid-latitudes and similar in shape for all 14 experiments. It is a positive geopotential height anomaly of  $6m$  amplitude, centered at mid-latitudes 30 degrees downstream to the SSTa center with identical spatial pattern. This component of the atmospheric column response is primarily driven by a warming of the lower layer (Fig.3-e-j). Given the vertical profile of heat flux forcing induced by the SSTa (restricted to the lower layer see Eq. (3)-(5)), this component of the response is related to the direct forcing of the SSTa.

[Figure 5 about here.]

<sup>1</sup>Given the fact that in this QG layer model, a temperature anomaly into a particular layer is related, via the thermal wind balance, to opposite geopotential height anomalies at the two pressure levels embedding the layer.

[Figure 6 about here.]

Barotropic mode responses are shown in Fig.(5) for SST-0E (plot A) and SST-180E (plot B) experiments. They exhibit two phases of a similar pattern made of a meridional dipole of geopotential height anomalies centered at mid-latitudes and over the Antarctic continent. This stationary pattern is similar to the SAM (Fig.2-D).

Figure 5-C illustrates how this result is persistent among the 14 experiments. It shows the spatial correlation between the barotropic mode responses and the SAM from the control simulation. Most of the correlations are greater than  $\pm 0.8$  and the two bands of longitude (shaded areas) where the transition between one phase and the other occurs are remarkably narrow compared to the domain size. This curve helped to determine the two different sets of experiments introduced in the previous section and illustrated in Fig.2-A. Figure 5-C also shows the meridional dipole amplitude ( $\Delta Z_{Bt}$ , see figure caption). It is larger in the first set of experiments (in the range  $[30; 50] m$ ) which project on a positive SAM phase than in the second set of experiments (in the range  $[-20; -30] m$ ).

Despite a strong zonally symmetric signature, barotropic geopotential height responses also contain zonally asymmetric structures. Departure from the zonal mean of  $Z_{Bt}$  are shown in Figure 6 plots A and B for SST-0E and SST-180E experiments and mid-latitudes averaged for all experiments in plot C. We'll refer to this component of the response as the barotropic quasi-stationary wave ( $QSW_{Bt}$ ). Fig. 6 shows that the  $QSW_{Bt}$  response is made of a zonal wavenumber one wave train propagating pole/westward with a positive geopotential height anomaly centered 50 to 60 degrees eastward of the SSTa forcing. This pattern is remarkably persistent among the 14 experiments (Fig.6-C). It is worth noting that a low pressure anomaly at 800hPa is not in contradiction with a local barotropic anomaly being positive. This means that the entire atmospheric air column is warming but not uniformly. Indeed the zonal asymmetric component of the vertical average temperature response, mean of 350hPa and 650hPa temperatures, is similar to the  $QSW_{Bt}$  response patterns (not shown). In the next section we show how the  $QSW_{Bt}$  pattern is crucial to understand the zonally symmetric response phase shift between the two sets of experiments.

#### 4. Potential vorticity balance leading to responses

In this section a simplified potential vorticity budget for each vertical mode of the response is conducted in order to understand which terms drive the PV balance and shape the stationary atmospheric responses.

Previous studies of atmospheric responses to SSTa have shown that in order to understand its physical mechanism it is crucial to separate the dynamics of transient eddies from those of quasi-stationary waves (Kushnir 1992; Kush-

nir et al. 2002; Ferreira and Frankignoul 2005). Consequently, we split the signal between high and low frequency components by use of a running mean. The cut-off frequency (the window width of the running mean) is set to 1/(7 days) and the signal decomposition written as:  $q_i = q'_i + q_i^*$  and  $\psi_i = \psi'_i + \psi_i^*$  where primes denote variability faster than 7 days (transient eddies) and stars the remaining signal. Introduced into Eqs.(3-4-5) in a steady state, this leads to:

$$0 = -[J(\psi_1^*, q_1^*)] - [J(\psi'_1, q'_1)] - [D_1] + S_1 \quad (8)$$

$$0 = -[J(\psi_2^*, q_2^*)] - [J(\psi'_2, q'_2)] - [D_2] + [Q_2] + S_2 \quad (9)$$

$$0 = -[J(\psi_3^*, q_3^*)] - [J(\psi'_3, q'_3)] - [D_3] + [Q_3] + S_3 \quad (10)$$

where  $[\cdot]$  stands for the long-term mean and we introduced  $Q_2 = -Q_{650}/K_b/R_b^2/C_{pa}$  and  $Q_3 = -Q_2$  for readability. We note that:

- i. This set of long-term mean PV balances holds for both perturbed and control runs.
- ii. Contributions from interactions between low and high frequency variability have been removed (even if they can be large at any time step, we verified *a posteriori* that their long-term mean is small compared to the other terms).
- iii. The balance contains non-linearities due to the convergence of quasi-stationary and eddy PV fluxes (first and second r.h.s. terms on (8)-(9)-(10)) but also in the tendency due to the diabatic heating because of the flow-dependent parametrization of the surface heat flux (see Eq.6).

Because the SSTa diabatic heating anomaly is a stretching of the lower layer, we also decomposed each PV convergence flux terms (the low and high frequency ones) into their relative vorticity ( $\zeta$ ) and vortex stretching ( $VS$ ) components as:  $J(\psi, q) = J(\psi, \zeta) + J(\psi, VS)$ .

These two decompositions (high vs low frequencies and relative vorticity vs vortex stretching PV convergence fluxes) multiply the number of terms to analyze at each pressure level. However, when projecting pressure levels responses onto vertical modes, interpretation of the results is simplified because PV budgets can be reduced to a few terms. Indeed, we found that relative vorticity terms primarily project themselves on the barotropic mode while vortex stretching ones project themselves, naturally, on the baroclinic modes. Thus the anomalous form (perturbed minus control fields) of PV balances (8)-(9)-(10) project on ver-

tical modes as (note that source terms  $S_i$  cancel):

$$0 = -[J(\psi^*, VS^*)]_{Bc1} - [J(\psi', VS')]_{Bc1} - [D]_{Bc1} + [Q]_{Bc1} \quad (11)$$

$$0 = -[J(\psi^*, VS^*)]_{Bc2} - [J(\psi', VS')]_{Bc2} - [D]_{Bc2} + [Q]_{Bc2} \quad (12)$$

$$0 = -[J(\psi^*, \zeta^*)]_{Bt} - [J(\psi', \zeta')]_{Bt} - [D]_{Bt} + H_{Bt} \quad (13)$$

where vertical modes interaction terms:

- are omitted in both baroclinic modes because we found *a posteriori* that they are unnecessary to the first order PV budget we want to investigate here,
- are represented by the new term  $H_{Bt}$  in the barotropic mode. This term is necessary because it is the only way for the SSTa to influence the barotropic mode in this 3 layers model where surface heat sources are localized in the lower layer only.  $H_{Bt}$  primarily represents baroclinic modes interactions (vertical propagation of anomalies).

Finally, each equation (11)-(12)-(13) is interpreted as an equilibrium between forcing and response terms which in turn are balanced by a damping – to ensure a closed and zero PV budget. In the following two sections we'll focus on the forcing/response terms equilibria, the one inducing a PV tendency responsible for geopotential height anomalies.

#### a. PV balance of baroclinic modes

Special attention needs to be paid to the heat flux term  $Q$  and therefore  $Q_{650}$  and  $F$ . The anomalous air-sea heat flux is a non linear combination of surface temperature and wind amplitude anomalies. These are in turn made of a direct forcing and an atmospheric response component. Using such a decomposition in surface variables would result in multiple heat flux components difficult to relate to a simple forcing/response equilibrium. Instead, we used a heat flux decomposition of the form

$$[F] = [F^{SST}] + [F^{ATM}], \quad (14)$$

where  $[F^{SST}]$  is the forcing component induced by the SSTa and  $[F^{ATM}]$  is the heat flux induced by atmospheric responses in surface temperature and wind. An estimate of the heat flux forcing term  $[F^{SST}]$  is obtained using mean fields of sea surface atmospheric air temperature and wind amplitude from the control simulation and SST fields with and without anomalies.

The  $[F^{ATM}]$  term is simply computed as the difference between the two other terms. It is a second order term in the main forcing/response balance in a sense that it is induced indirectly by the SSTa through the effect of the atmospheric response. In other words, it is a consequence

of the initial atmospheric response instead of the direct SSTa forcing.  $[F^{ATM}]$  is driven by positive temperature anomalies in the lower layer, see Fig.3-e-j. It is therefore negative (warming the ocean) and very close in shape to  $T(650hPa)$  (not shown). It has a 14 experiments ensemble mean of  $-5 W m^{-2}$  (corresponding to a heating rate of  $-0.10 K day^{-1}$  at 650hPa) with values between  $-10$  and  $-3 W m^{-2}$  in the Western Pacific and Atlantic-Western Indian Oceans ( $-0.19$  and  $-0.06 K day^{-1}$ ). In a coupled model, this component of the heat flux anomaly would help sustain the SSTa and increase its persistence. This is indeed what was shown by M06. Here it tends to moderate the amplitude of the direct atmospheric response, reducing the stretching between layers, and will therefore be omitted.

Using (14) to decompose heat sources at pressure level  $Q_{2,3} = \pm Q_{650}/K_b/R_b^2/C_{pa}$  and for baroclinic modes  $[Q]_{Bci}$ , we can write:

$$[Q^{SST}]_{Bci} - [J(\psi^*, VS^*)]_{Bci} - [J(\psi', VS')]_{Bci} \propto [q_{Bci}] \quad (15)$$

for  $i = 1, 2$  and where  $[q_{Bci}]$  are the baroclinic PV responses shown as geopotential heights in Fig.(4). All l.h.s. terms of (15) and their sum are shown for experiments SST-0E (left columns) and SST-180E (right columns) in Fig.7 for baroclinic mode 1 and Fig.8 for baroclinic mode 2. We now describe these patterns.

[Figure 7 about here.]

[Figure 8 about here.]

The baroclinic heat source forcing  $[Q^{SST}]_{Bci}$  has the SSTa pattern but sees its amplitude varying according to zonal asymmetries in surface atmospheric fields. It has a 14 experiments ensemble mean amplitude of  $24 W m^{-2}$  (and a corresponding heating rate at 650hPa of  $0.45 K day^{-1}$ ) with values between  $15$  and  $31 W m^{-2}$  (heating rate between  $0.28$  and  $0.59 K day^{-1}$  at 650hPa) in the Western Pacific and Atlantic-Western Indian Oceans.

The baroclinic quasi-stationary vortex stretching flux  $-[J(\psi^*, VS^*)]_{Bci}$  exhibits a zonal dipole in the midlatitude band, centered around 30 degrees downstream of the SSTa center, reminiscent of an advective pattern. The negative (positive) vortex stretching anomaly induced by the SSTa in the 1<sup>st</sup> (2<sup>nd</sup>) baroclinic mode is clearly advected eastward by the the quasi-stationary flow. Contributions from the stationary flow is dominant upon the low-frequency one in this advection pattern (not shown). Like geopotential height responses, their amplitudes are larger in the SST-0E case than in the SST-180E one. And not surprisingly, these tendency patterns are very similar among the 14 experiments with regard to their relative positions to SSTa forcing longitude.

The baroclinic high frequency eddy vortex stretching flux  $-[J(\psi', VS')]_{Bci}$  is of the opposite sign of the vortex stretching anomaly at the latitude of the SSTa forcing and of the same sign north and southward of it, with a relatively small zonal asymmetry. This term thus plays a dissipative role in the balance. It dissipates in the meridional direction the anomalous vortex stretching induced by the SSTa and again, no differences are found between experiments except in the amplitude. The anomalous vortex stretching induced by the SSTa increases the available potential energy of the atmospheric column which tends to be released through baroclinic instability, i.e. by an increase of the baroclinic transients activity. They induce a divergence of eddy temperature flux in the latitude band of the SSTa and a convergence on its north/south flanks which explain the pattern of  $-[J(\psi', VS')]_{Bci}$ .

The sum of all terms shows a geopotential height tendency pattern close to the baroclinic responses shown in Fig.4. The warm atmospheric temperature response, shifted eastward from the SSTa forcing longitude, is well explained by a simple equilibrium between the SSTa direct forcing and (i) advection from the quasi-stationary flow and (ii) dissipation by the high frequency transient eddies. This balance holds in the vicinity of the SSTa, from its longitude center up to 90 degrees eastward. For the 14 experiments we observed baroclinic responses similar with regard to their relative distribution to the SSTa forcing position. This is also true for the baroclinic PV balance terms shaping the response pattern. However, the simplified PV budget of the 1<sup>st</sup> baroclinic mode is not able to explain the different sign of geopotential height anomalies observed over the South Pole in experiments SST-0E and SST-180E. Such a discrepancy from the budget and the observed responses probably arises from the error accumulation of all decompositions.

#### b. PV balance of the barotropic mode

The barotropic PV budget (13) is quantitatively harder to tackle than the baroclinic ones because of the unknown forcing term  $H_{Bt}$ . While baroclinic modes are almost directly forced by the SSTa – and a direct diagnostic is possible – the barotropic mode response necessary involves the integrated (both vertically and over time) effect of the vertical propagation of anomalies. This is simply because the vertical integral of the discretized heat sources in (3)-(5) is zero. Thus the barotropic response must be forced by anomalies in surface boundary conditions diagnosed from anomalous baroclinic heat sources. We choose not to conduct this diagnostic of  $H_{Bt}$  because it involves multiple complicated and convoluted scalings to transform the vertically averaged atmospheric temperature response into an anomalous surface heat flux suited for a barotropic atmosphere. However, we show hereafter that a qualitative discussion of  $H_{Bt}$  with analysis of the other terms from (13)

is satisfactory enough to explain the pattern and behavior of the atmospheric barotropic responses. In other words, in this sequence of experiments the qualitative knowledge of the forcing is sufficient to the comprehension of the forcing/response equilibria.

In section 3 we show that the lower and upper layers of the atmosphere warm eastward of the SSTa (see Fig.4 and Eq.A5 for instance). This reflects a warming of the entire air column – a barotropic warm air anomaly – although not with an uniform distribution along the vertical axis. When this warming projects at the surface, it modifies the boundary conditions of the equivalent barotropic atmosphere and can force the barotropic mode response. More precisely, here it forces a local downstream high pressure anomaly (because the entire air column warming makes geopotential height surfaces move upward) which in turn excites a planetary Rossby wave train. This is indeed what is seen in the barotropic quasi-stationary wave responses (Fig.6). The  $QSW_{Bt}$  atmospheric response turns out to be a proxy of the  $H_{Bt}$  forcing pattern and is induced by a simple local warming of the entire air column.

How then can the different projections on the SAM phase be explained ?

Figure 9 shows zonal anomalies of  $-[J(\psi^*, \zeta^*)]_{Bt}$  and  $-[J(\psi', \zeta')]_{Bt}$  for SST-0E and SST-180E experiments. We can see that the high pressure anomaly from the barotropic forcing term  $H_{Bt}$  is (i) balanced by a low pressure anomaly induced by the convergence of quasi-stationary relative vorticity fluxes (plots A and B) and (ii) slightly reinforced by the eddy component of the relative vorticity flux (plots C and D). For all 14 experiments, these patterns of zonal anomalies are phase locked with the SSTa forcing longitude similarly to  $QSW_{Bt}$  responses.

The zonal mean of  $-[J(\psi^*, \zeta^*)]_{Bt}$  and  $-[J(\psi', \zeta')]_{Bt}$  are shown Fig.(9) plots E and F. The eddy  $\zeta$  flux (thick dashed line) is negligible over the South Pole and made of a dipole at mid-latitudes with convergence to the south and divergence to the north of the SSTa latitude, simply revealing an extremum of high frequency eddy structures at this latitude. For experiment SST-0E (plot E), the quasi-stationary  $\zeta$  flux (thick solid line) is a meridional dipole with large negative (positive) values over the South Pole (at mid-latitudes) which compare well to the meridional structure of the  $SAM_{Bt}$  zonal mean in a positive phase and to the  $Z_{Bt}$  zonal mean response (not shown but illustrated in Fig.5). For experiment SST-180E (plot F) we observe a similar structure and correlation with a negative phase of the  $SAM_{Bt}$ .

This is evidence that  $-[J(\psi^*, \zeta^*)]_{Bt}$  drives the sign of the geopotential height response projection on the  $SAM_{Bt}$  pattern. Indeed, the low frequency eddy - mean flow interaction process, here captured by the  $-[J(\psi^*, \zeta^*)]_{Bt}$  term, is partially responsible for the meridional structure of the zonal mean zonal velocity field ( $\partial_t u \propto -\partial_y u^* v^*$ ). Zonal

asymmetries in the time mean flow arise from zonal anomalies in surface boundary conditions. As one can see from Fig.2-C, the control quasi-stationary wave pattern has a zero contour at the SSTa forcing latitude flanked to the north/south of (i) high/low pressure anomalies from Drake Passage to the Western Indian Ocean and (ii) low/high pressure anomalies from South of Australia to the Mid-Pacific Ocean. The downstream high pressure anomaly from the  $QSW_{Bt}$  response thus modifies the meridional high/low pressure distribution of the control wave (shifting south or northward the control high pressure anomaly) and hence the meridional structure of the zonal mean flow through low frequency relative vorticity fluxes. Having zonal asymmetries in the control state and a perturbed low frequency eddy field locked with the SSTa forcing longitude, induces the possibility for the perturbed flow to reinforce or weaken eddy-mean flow interactions and to project responses on positive/negative phases of the dominant zonal mean flow pattern.

[Figure 9 about here.]

## 5. Discussion

An analysis of 14 experiments where an atmospheric QG model was forced by an idealized SSTa centered at mid-latitudes and 14 different longitudes was presented. We focused on the vertical structures of stationary responses by projecting pressure level anomalies onto the three vertical modes of the model. One obtained a barotropic component and two baroclinic modes representing the vertical distribution of layer stretching. Results are illustrated by schematics on figure 6.

We found that the two baroclinic modes and the zonal anomaly of the barotropic one ( $QSW_{Bt}$ ) are insensitive to the SSTa location in the sense that they are zonally phase locked with the SSTa forcing position. On the other hand, zonal average responses show a SAM like pattern with a phase highly sensitive to the SSTa location: positive for a forcing centered from the Drake passage to the Western Indian Ocean and negative for a forcing centered between South of Australia and the Mid-Pacific Ocean.

Baroclinic modes anomalies – warm air anomalies in the lower and upper layers – have basically the SSTa forcing pattern shifted downstream, eastward, by about 40-50 degrees (Fig.4). These types of baroclinic responses have long been observed in the North Atlantic and the North Pacific regions (Ting and Peng 1995; Peng and Whitaker 1999). Their dynamical balance is schematically illustrated in Fig.6, plots A and B. Using an approximated potential vorticity budget we determined that baroclinic responses can largely be explained by the anomalous vortex stretching induced by the SSTa being balanced by (i) advection by the quasi-stationary flow (dominated by the stationary part, not shown) and (ii) dissipation by the mean tran-

sients effect. We also determined that the amplitude of these baroclinic mode structures is linearly proportional to the SSTa amplitude for anomalies up to  $\pm 4^{\circ}\text{C}$  (not shown) with the lower layer atmospheric temperature anomaly about 70% the SSTa amplitude. We didn't compare our results to a classic Linear Baroclinic Model experiment (e.g., Peng et al. 2003), but these elements seem to agree with the linear QG theory (Smagorinsky 1953; Hoskins and Karoly 1981; Frankignoul 1985).

Although the heat anomaly is not uniformly distributed throughout the vertical, all stationary responses show a warming of the entire air column 40 to 50 degrees downstream of the SSTa (Fig.6-C). This barotropic warming induces a high pressure anomaly simply through rising geopotential height surfaces which in turn excite a barotropic quasi-stationary Rossby wave train propagating pole/westward and of zonal wave number one (see Fig.6). The amplitude of the  $QSW_{Bt}$  response, from 4 to 10m, is about 10% the amplitude of the control field (from 60m at mid-latitudes to 100m around the Pole). It is worth noting that having a downstream low pressure anomaly response at 800hPa – and one would expect a similar surface pressure response – is not in contradiction with a barotropic downstream high pressure anomaly.

The simplified control  $QSW_{Bt}$  pattern is schematically represented in Fig.6-D (see Fig.2-C for more details). It has a zero contour at the SSTa forcing latitude flanked to the north/south of (i) high/low pressure anomalies from Drake Passage to the Western Indian Ocean and (ii) low/high pressure anomalies from South of Australia to the Mid-Pacific Ocean. The sensitivity of the zonal mean response phase to the SSTa forcing position is due to this pattern. Indeed, the downstream high pressure anomaly from the  $QSW_{Bt}$  response modifies the meridional high/low pressure distribution in opposite ways, depending on where the SSTa forcing is localized (see Fig.6-D for the SST-0E and SST-180E experiments). Diagnosing low and high frequency relative vorticity eddy fluxes, we have shown that it is the low frequency eddy component which is responsible for the modified eddy-mean flow interaction leading to different responses.

In the reality the high frequency eddy component plays a much significant role in eddy-mean flow interactions of the Southern Hemisphere (see Watterson 2002, for instance). It is possible that we obtain this result because the bottom friction time scale used in the model (from 1.5 to 3 days, depending on topography) is too short compared to observations (Watterson 2007, found 8.6 days as effective time) and hence high frequency eddies are damped too quickly. If the damping is decreased (i.e., with a longer timescale), the model should also produce responses less localized to the forcing – with stronger eastward propagation – and with larger amplitudes which could alter low/high frequency eddy interactions with the mean flow. Seasonality may

also play a role even if observed damping time scales are shorter in winter – the season modeled here – than in summer (Watterson 2002).

Finally, it is remarkable that we obtained such a simple zonal mean response behavior with respect to the SSTa forcing position (same pattern, two phases). Our study suggests that a warming of the mid-latitudes Southern Ocean is likely to have two opposite impacts on the SAM depending on the warming position: positive for Atlantic to West-Indian Oceans warming and negative for South of Australia to Mid-Pacific Oceans warming. As a consequence, this also suggests that it may be possible to enhance a trend in the SAM through warming of distinct regions of the Southern Ocean.

[Figure 10 about here.]

## 6. Conclusion

Using a 3-level quasi-geostrophic atmospheric model forced by the ocean through a diabatic heat source in the lower layer, we determined the stationary atmospheric response to an idealized SST anomaly in the Southern Ocean in perpetual winter conditions. While in many past studies atmospheric responses to SST anomalies had been analyzed in simple zonally symmetric models mimicking the Southern Hemisphere (e.g. Inatsu et al. 2003; Ring and Plumb 2007) this study takes into account asymmetries both in the high-frequency and low-frequency atmospheric variability (storm-track and quasi-stationary eddies). This study suggests that, albeit small compared to their Northern Hemisphere counterpart, these asymmetries play a crucial role in determining the large-scale atmospheric response to a SST anomaly in the Southern Hemisphere.

Further investigations are needed to check at the robustness of these results in more complex atmospheric models. In particular it is necessary to clarify the influence of (i) the friction parametrization, using different dissipation time scales both in the bottom friction and the layer radiative coupling, (ii) the background state and especially the seasonality of the quasi-stationary wave pattern, and (iii) the vertical profile of the heat source, extending the vertical penetration of heat to the upper layer.

To conclude, we have shown that a SSTa transported by the ACC can impact the overlying atmosphere. Baroclinic and barotropic zonal anomalies responses are phased locked with the SSTa forcing position, shifted downstream by about 50 degrees. These responses could feedback on the SSTa through anomalous zonal winds modifying oceanic currents and/or air-sea fluxes.

And finally, we also have shown that the SAM is sensitive to mid-latitudes SSTa. The zonal mean barotropic response is either reinforcing or weakening a SAM like pattern depending on the localization of the SSTa forcing with respect to the control quasi-stationary wave. Whether mid-

latitudes Southern Ocean warming trends (as those observed by Gille et al. 2001, for instance) could contribute to the observed SAM trend will require complementary studies using more realistic models. Our study, with caution, suggests that the mid-latitudes Southern Ocean may also play a role in driving climatic trends in the Southern Hemisphere atmosphere.

*Acknowledgments.*

Authors are thankful for discussions with D. Ferreira and C. Frankignoul. We also thank I. Watterson and two anonymous reviewers for their useful and constructive comments.

APPENDIX

7. Source terms

The usual way to compute source terms  $S_i$  in PV equations give better results applied to Southern Hemisphere when corrected with a fixed temperature profile. This term was computed in the following way.

The Marshall and Molteni (1993) forcing term  $S_i$  can be interpreted as a relaxation temperature in the sense of Held and Suarez (1994). Eqs.(3-5) can in fact be obtained eliminating the vertical velocity  $\omega$  in the QG vorticity and temperature equations (compare Holton 1992, p.164):

$$\frac{d\nabla^2\psi}{dt} = f_0 \frac{\partial\omega}{\partial p} \quad (\text{A1})$$

$$f_0 \frac{d\psi}{dt} = -\sigma\omega + F(\psi, T) + \frac{R}{p} \frac{1}{\tau} (T^* - T) \quad (\text{A2})$$

Which gives

$$\frac{Dq}{Dt} = \frac{f_0}{\sigma} \frac{\partial}{\partial p} F(\psi, T) - \frac{f_0}{\sigma} \frac{1}{\tau} \frac{\partial}{\partial p} \left[ \frac{R}{p} T \right] + \frac{f_0}{\sigma} \frac{1}{\tau} \frac{\partial}{\partial p} \left[ \frac{R}{p} T^* \right] \quad (\text{A3})$$

Here,  $q$  is the potential vorticity,  $\psi$  the geostrophic streamfunction,  $f_0$  the Coriolis factor at  $45^\circ S$ ,  $\sigma$  the static stability,  $R$  the gas constant and  $\tau$  a relaxation time scale. The first term on the r.h.s. of Eq.(A3) corresponds to the heat flux term in Eqs.(4-5). The second term on the r.h.s. of Eq.(A3) corresponds to the dissipation term of Eqs.(3-5). Finally, the third term represents the Held and Suarez relaxation temperature.

The Marshall and Molteni (1993) forcing method, in other terms, can be seen as an empirical way to compute a relaxation temperature  $T^*$ .

In order to correct the forcing term  $S$ , we added a zonally uniform temperature  $T^{*'}$  and recomputed a new term  $S'$ :

$$S' = \frac{f_0}{\sigma} \frac{1}{\tau} \frac{\partial}{\partial p} \left[ \frac{R}{p} (T^* + T^{*'}) \right] \quad (\text{A4})$$

where  $T^{*'}$  is pretty much an *ad hoc* term, it was computed as a fraction of the difference in meridional profile between  $T^*$  and the observed meridional temperature profile.

APPENDIX

8. Vertical modes

As the model is discretized at 3 pressure levels, it can be projected on three vertical modes, one barotropic and two baroclinic. These are defined as the eigenvectors of the transfer matrix  $\mathbf{T}$ , defined by the vortex stretching term of the transformation of the streamfunctions  $\psi$  into the potential vorticities  $q$  :

$$\begin{pmatrix} q_{200} \\ q_{500} \\ q_{800} \end{pmatrix} = \mathbf{T} \begin{pmatrix} \psi_{200} \\ \psi_{500} \\ \psi_{800} \end{pmatrix} \quad (\text{A1})$$

where  $\mathbf{T}$  is defined as:

$$\mathbf{T} = \begin{pmatrix} -\frac{1}{R_h^2} & \frac{1}{R_h^2} & 0 \\ \frac{1}{R_h^2} & -\frac{1}{R_h^2} - \frac{1}{R_b^2} & \frac{1}{R_b^2} \\ 0 & \frac{1}{R_b^2} & -\frac{1}{R_b^2} \end{pmatrix} \quad (\text{A2})$$

with  $R_h = 700km$  and  $R_b = 450km$  the Rossby radius of deformation of the upper and lower layers of the model (see Fig.1). Then vertical modes of a variable defined at each pressure levels (potential vorticity, streamfunction or geopotential height  $z$  as followed) are obtained through the inversion of:

$$\begin{pmatrix} z_{200} \\ z_{500} \\ z_{800} \end{pmatrix} = \mathbf{M} \begin{pmatrix} z_{Bt} \\ z_{Bc1} \\ z_{Bc2} \end{pmatrix} \quad (\text{A3})$$

where indices  $Bt$ ,  $Bc1$  and  $Bc2$  stand for the barotropic and first, second baroclinic modes and the matrix  $M$  contains the eigen vectors of the transfer matrix  $\mathbf{T}$ . This can be numerically approximated by:

$$\begin{pmatrix} z_{Bt} \\ z_{Bc1} \\ z_{Bc2} \end{pmatrix} \simeq \begin{pmatrix} 0.57 & 0.57 & 0.57 \\ -0.79 & 0.25 & 0.54 \\ -0.17 & 0.77 & -0.6 \end{pmatrix} \begin{pmatrix} z_{200} \\ z_{500} \\ z_{800} \end{pmatrix} \quad (\text{A4})$$

Note that given the thermal wind relation in each layers, vertical baroclinic modes of geopotential height may be related to temperatures at 350hPa and 650hPa through:

$$\begin{pmatrix} z_{Bc1} \\ z_{Bc2} \end{pmatrix} \simeq \begin{pmatrix} -21.41 & -7.54 \\ -4.60 & 8.33 \end{pmatrix} \begin{pmatrix} T_{350} \\ T_{650} \end{pmatrix} \quad (\text{A5})$$

REFERENCES

Butler, A. H., D. W. J. Thompson, and R. Heikes, 2010: The steady-state atmospheric circulation response to climate change-like thermal forcings in a simple general circulation model. *Journal of Climate*, **23** (13), 3474–3496, doi:10.1175/2010JCLI3228.1

- Codron, F., 2007: Relations between annular modes and the mean state: Southern hemisphere winter. *Journal of the Atmospheric Sciences*, **64** (9), 3328–3339, doi:10.1175/JAS4012.1
- Connolley, W., 2002: Long-term variation of the Antarctic Circumpolar Wave. *J. Geophys. Res.*, **107**.
- Czaja, A. and C. Frankignoul, 2002: Observed impact of Atlantic sst anomalies on the North Atlantic oscillation. *J. Climate*, **15** (6), 606–623.
- D’Andrea, F., A. Czaja, and J. Marshall, 2005: Impact of anomalous ocean heat transport on the North Atlantic oscillation. *J. Climate*, **18**, 4955–4969, doi:10.1034/j.1600-0870.2000.520103.x
- D’Andrea, F. and R. Vautard, 2000: Reducing systematic errors by empirically correcting model errors. *Tellus*, **52A**, 21–41, doi:10.1034/j.1600-0870.2000.520103.x
- Ferreira, D. and C. Frankignoul, 2005: The transient atmospheric response to midlatitude sst anomalies. *J. Climate*, **18**, 1049–1067, doi:10.1175/JCLI-3313.1.
- Ferreira, D. and C. Frankignoul, 2008: Transient atmospheric response to interactive sst anomalies. *J. Climate*, **21** (3), 576–583.
- Frankignoul, C., 1985: Sea surface temperature anomalies, planetary waves, and air-sea feedback in the middle latitudes. *Review of Geophysic*, **23** (4), 357–390.
- Gibson, R., P. K allberg, and S. Uppala, 1996: The ecmwf re-analysis (era) project. Tech. Rep. 73, ECMWF Newsletter, 7-17 pp.
- Gille, S. T., D. P. Stevens, R. T. Tokmakian, and K. J. Heywood, 2001: Antarctic circumpolar current response to zonally averaged winds. *J. Geophys. Res.*, **106**, 273–2759.
- Gillett, N. P. and D. W. J. Thompson, 2003: Simulation of recent Southern hemisphere climate change. *Science*, **302** (5643), 273–275.
- Grassi, B., G. Redaelli, and G. Visconti, 2005: Simulation of polar antarctic trends: Influence of tropical sst. *Geophys. Res. Lett.*
- Hall, A. and M. Visbeck, 2002: Synchronous variability in the Southern hemisphere atmosphere, sea ice, and ocean resulting from the annular mode. *J. Climate*, **15**, 3043–3057, doi:10.1175/1520-0442(2002)015<3043:SVITSH>2.0.CO;2
- Hall, N. M. J., J. Derome, and H. Lin, 2001: The extratropical signal generated by a midlatitude sst anomaly. part i: Sensitivity at equilibrium. *J. Climate*, **14**, 2035–2053.
- Hartmann, D. L. and F. Lo, 1998: Wave-driven zonal flow vacillation in the Southern hemisphere. *Journal of the Atmospheric Sciences*, **55**, 1303–1315, doi:10.1175/1520-0469(1998)055<1303:WDZTFVI>2.0.CO;2.
- Held, I. and M. Suarez, 1994: A proposal for the intercomparison of the dynamical cores of atmospheric general circulation models. *Bulletin of the American Meteorological Society*, **75**, 1825–1830.
- Holton, J. R., 1992: *An Introduction to dynamic Meteorology*. Academic Press.
- Hoskins, B. and D. Karoly, 1981: The steady linear response of a spherical atmosphere to thermal and orographic forcing. *Journal of the Atmospheric Sciences*, **38**, 1179–1196.
- Inatsu, M., H. Mukougawa, and S.-P. Xie, 2003: Atmospheric response to zonal variations in midlatitude sst: Transient and stationary eddies and their feedback. *J. Climate*, **16**, 3314–3329, doi:10.1175/1520-0442(2003)016<3314:ARTZVI>2.0.CO;2.
- Kidson, J., 1988: Indices of the Southern hemisphere zonal wind. *J. Climate*, **1**, 183–194.
- Kravtsov, S., J. E. Ten Hoeve, S. B. Feldstein, S. Lee, and S.-W. Son, 2009: The relationship between statistically linear and nonlinear feedbacks and zonal-mean flow variability in an idealized climate model. *Journal of the Atmospheric Sciences*, **66** (2), 353–372, doi:10.1175/2008JAS2804.1.
- Kushnir, Y., 1992: The general circulation model response to a North Pacific sst anomaly: Dependence on timescale and pattern polarity. *J. Climate*, **5**, 271–283.
- Kushnir, Y., W. A. Robinson, I. Blad , N. M. J. Hall, S. Peng, and R. Sutton, 2002: Atmospheric gcm response to extratropical sst anomalies: Synthesis and evaluation. *J. Climate*, **15**, 2233–2256.
- Li, S., J. Perlwitz, M. P. Hoerling, and X. Chen, 2010: Opposite annular responses of the northern and southern hemispheres to indian ocean warming. *Journal of Climate*, **23** (13), 3720–3738, doi:10.1175/2010JCLI3410.1.
- Marshall, J. and F. Molteni, 1993: Toward a dynamical understanding of planetary-scale flow regimes. *Journal of the Atmospheric Sciences*, **50** (12), 1792–1818.
- Maze, G., 2006: Ocean-atmosphere low-frequency interactions in the southern ocean. Ph.D. thesis, Universit  Paris VI, 130 pp. [Available at: <http://www.guillaumemaze.org/research/phd>]

- Maze, G., F. D’Andrea, and A. Colin de Verdière, 2006: Low-frequency variability in the Southern ocean region in a simplified coupled model. *J. Geophys. Res.*, **111** (C05010), doi:10.1029/2005JC003181.
- Minobe, S., A. Kuwano-Yoshida, N. Komori, S.-P. Xie, and R. J. Small, 2008: Influence of the gulf stream on the troposphere. *Nature*, **452** (7184), 206–209.
- Peng, S., W. Robinson, and S. Li, 2003: Mechanisms for the NAO responses to the North Atlantic sst tripole. *J. Climate*, **16**, 1987–2004.
- Peng, S. and W. A. Robinson, 2001: Relationships between atmospheric internal variability and the responses to an extratropical sst anomaly. *J. Climate*, **14**, 2943–2959.
- Peng, S. and J. S. Whitaker, 1999: Mechanisms determining the atmospheric response to midlatitude sst anomalies. *J. Climate*, **12**, 1393–1408.
- Perlwitz, J., S. Pawson, R. L. Fogt, J. E. Nielsen, and W. D. Neff, 2008: Impact of stratospheric ozone hole recovery on Antarctic climate. *Geophys. Res. Lett.*, **35** (8).
- Reynolds, R. and T. Smith, 1994: Improved global sea surface temperature analyses using optimum interpolation. *J. Climate*, **7**, 929–948.
- Ring, M. J. and R. A. Plumb, 2007: Forced annular mode patterns in a simple atmospheric general circulation model. *Journal of the Atmospheric Sciences*, **64** (10), 3611–3626.
- Roads, J. O., 1987: Predictability in the extended range. *Journal of the Atmospheric Sciences*, **44**, 3495–3527.
- Rodwell, M. and C. Folland, 2002: Atlantic air-sea interaction and seasonal predictability. *Quart. J. Roy. Meteor. Soc.*, **31** (583), 1413–1443.
- Simmonds, I., 2003: Modes of atmospheric variability over the southern ocean. *J. Geophys. Res.*, **108** (C4).
- Smagorinsky, J., 1953: The dynamical influence of large-scale heat sources and sinks on the quasi-stationary mean motions of the atmosphere. *Quart. J. Roy. Meteor. Soc.*, **79**, 342–366.
- Son, S.-W. and S. Lee, 2005: The response of westerly jets to thermal driving in a primitive equation model. *Journal of the Atmospheric Sciences*, **62** (10), 3741–3757, doi:10.1175/JAS3571.1.
- Thompson, D. W. and J. Wallace, 1998: The arctic oscillation signature in the wintertime geopotential height and temperature fields. *Geophys. Res. Lett.*, **25**, 1297–1300.
- Thompson, D. W. and J. M. Wallace, 2000: Annular modes in the extratropical circulation. part i: Month-to-month variability. *J. Climate*, **13**, 1000–1016.
- Thompson, D. W. J. and S. Solomon, 2002: Interpretation of recent Southern hemisphere climate change. *Science*, **296** (5569), 895–899.
- Ting, M. and S. Peng, 1995: Dynamics of the early and middle winter atmospheric responses to the NorthWest Atlantic sst anomalies. *J. Climate*, **8** (9), 2239–2254.
- Verdy, A., J. Marshall, and A. Czaja, 2006: Sea surface temperature variability along the path of the antarctic circumpolar current. *Journal of Physical Oceanography*, **36** (7), 1317–1331.
- Watterson, I. G., 2000: Southern midlatitude zonal wind vacillation and its interaction with the ocean in gcm simulations. *Journal of Climate*, **13** (3), 562–578.
- Watterson, I. G., 2001: Zonal wind vacillation and its interaction with the ocean: Implications for interannual variability and predictability. *J. Geophys. Res.*, **106** (D20), 23 965–23 975.
- Watterson, I. G., 2002: Wave–mean flow feedback and the persistence of simulated zonal flow vacillation. *Journal of the Atmospheric Sciences*, **59** (7), 1274–1288.
- Watterson, I. G., 2007: Southern “annular modes” simulated by a climate model—patterns, mechanisms, and uses. *Journal of the Atmospheric Sciences*, **64** (9), 3113–3131, doi:10.1175/JAS4014.1.
- Watterson, I. G., 2010: Relationships between south-eastern australian rainfall and sea surface temperatures examined using a climate model. *J. Geophys. Res.*, **115** (D10).
- White, W. B., 2004: Comments on ‘synchronous variability in the Southern hemisphere atmosphere, sea ice, and ocean resulting from the annual mode. *J. Climate*, **17**, 2249–2254.

## List of Figures

1	Schematic of the vertical discretization of the model. . . . .	14
2	Experiments set-up and control run climatology. . . . .	15
3	Stationary atmospheric responses at pressure levels. . . . .	16
4	Vertical structure of responses: Baroclinic modes. . . . .	17
5	Vertical structure of responses: Barotropic mode. . . . .	18
6	Vertical structure of responses: Zonal assymetries in the barotropic mode. . . . .	19
7	PV balance of the 1 <sup>st</sup> baroclinic mode. . . . .	20
8	PV balance of the 2 <sup>nd</sup> baroclinic mode. . . . .	21
9	PV balance of the barotropic baroclinic mode. . . . .	22
10	Schematic of the results. . . . .	23

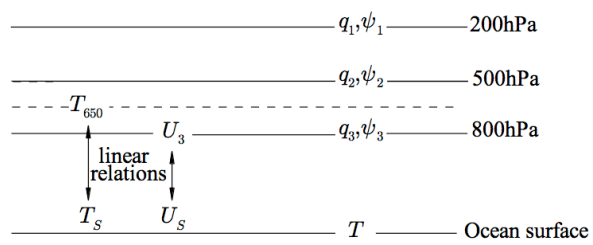


FIG. 1. Schematic of the vertical discretization of the model.

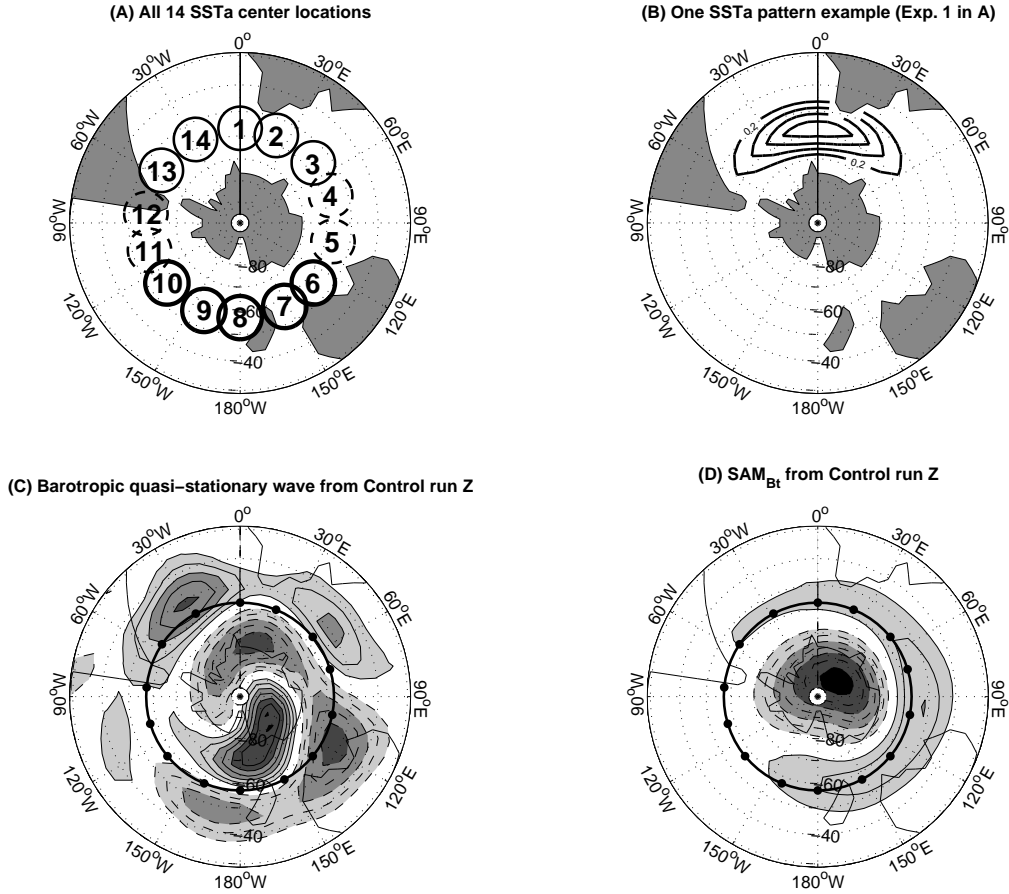


FIG. 2. Plot A: Locations of the SSTA center for the 14 experiments. They are 3 types of circle symbol: light or heavy solid for barotropic responses projecting on a positive or negative SAM phase and light dashed for intermediate cases, see text for more details. Plot B: SSTA pattern centered at  $0^{\circ}E$  with a  $1^{\circ}C$  amplitude. Contours every  $0.2^{\circ}C$ . Plot C: Quasi-stationary wave of the control simulation from the geopotential height barotropic component (departure from the zonal mean of the time mean 7 days low-pass filtered field). Contours every  $20m$ , negative dashed and zero contour omitted. Plot D: Barotropic component of the Southern Annular Mode for the control simulation (contours  $20m$ , negative dashed and zero contour omitted). The SAM is defined as the first principal component of monthly geopotential height anomalies. On plots C and D shading is based on magnitude and the heavy black line recalls the latitude circle ( $47^{\circ}S$ ) of all SSTA also indicated by the dots.

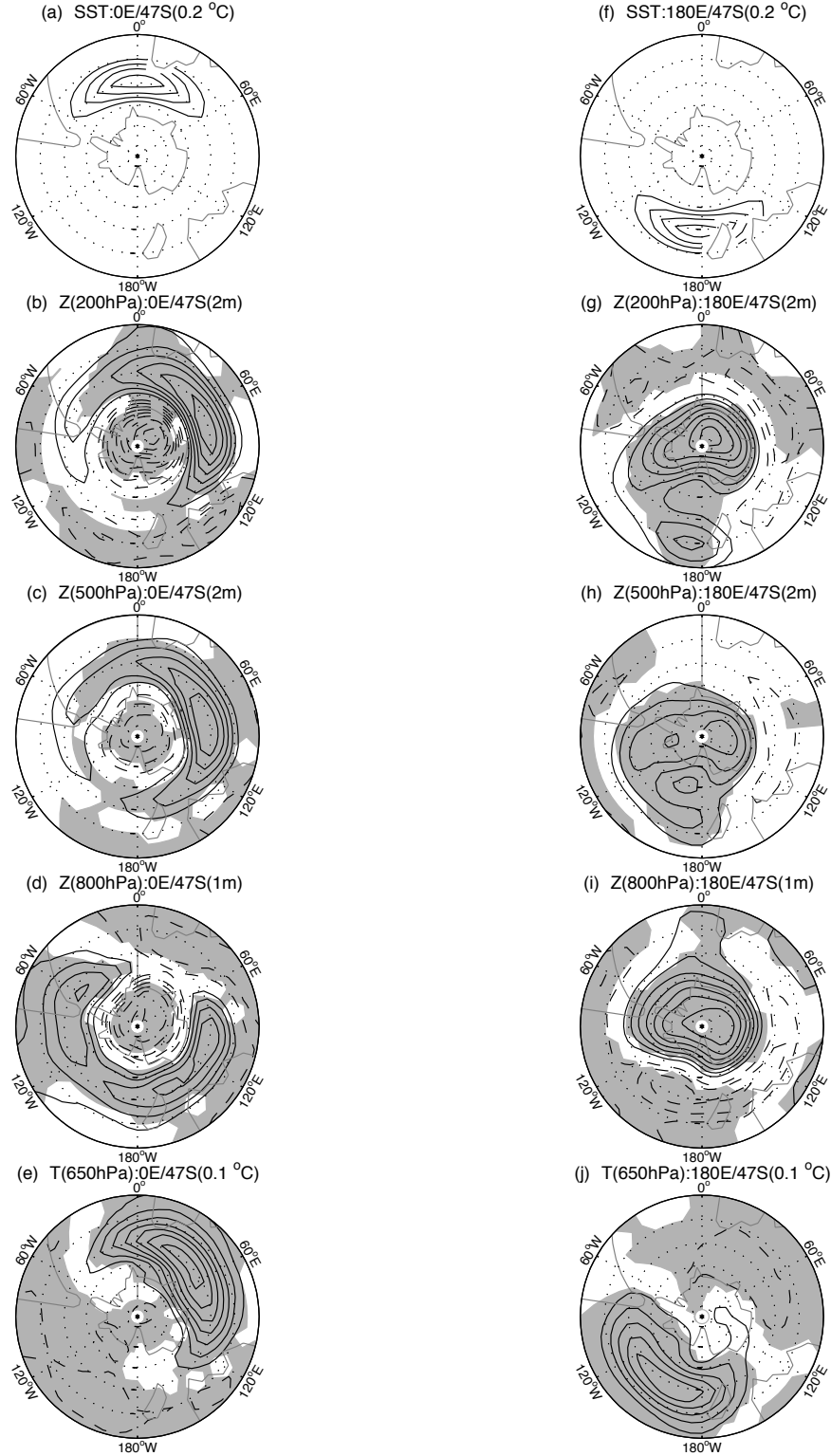


FIG. 3. Stationary atmospheric responses to an idealized SST anomalies of 1K amplitude (a and f) centered at  $47^{\circ}S$  and 0E (left column) and 180E (right column). Geopotential height responses at 200hPa are shown in plots b and g; at 500hPa in c and h; at 800hPa in d and i. Responses of atmospheric temperature at 650 hPa are shown in plots e and j. Zero contours omitted on all plots, contours interval is indicated in parenthesis in the panels subtitles. Gray shaded areas indicate the 95% significance level (not shown on SSTa plots a and f).

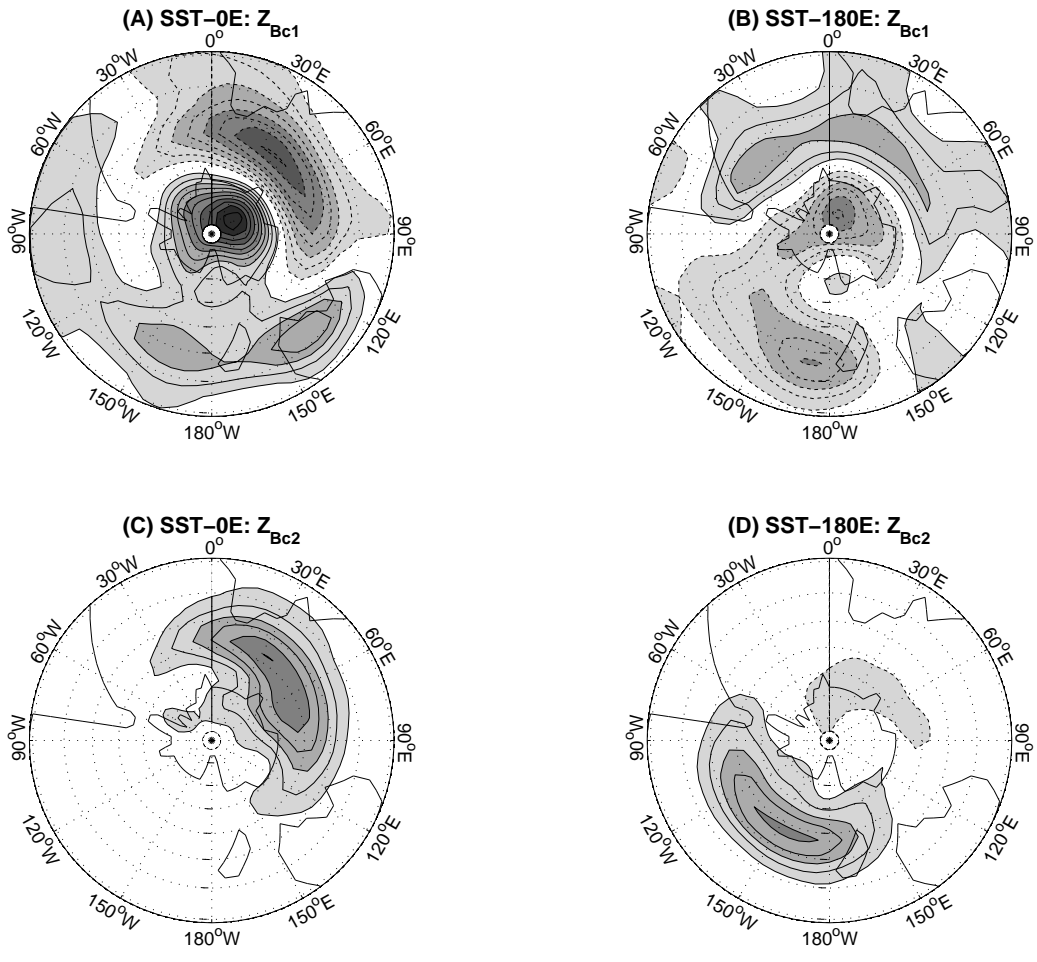


FIG. 4. Stationary atmospheric responses of geopotential height for SST-0E (left) and SST-180E (right) experiments projected on the first (top) and second (bottom) baroclinic vertical mode. Contours are every meters, negative contours are dashed, zero contour is omitted. Shading is based on magnitude.

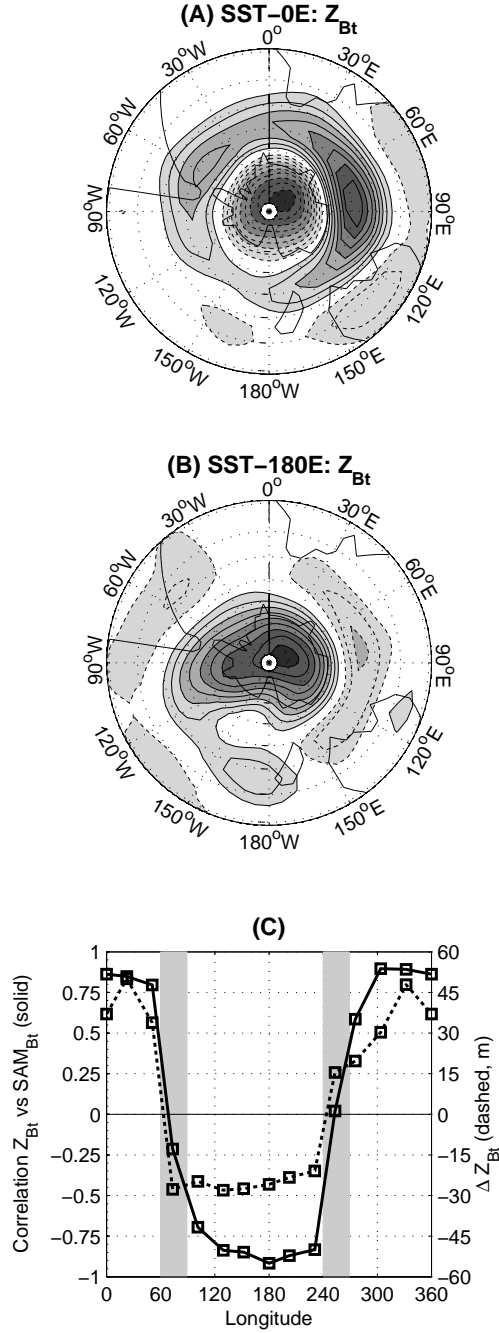


FIG. 5. Plots A-B: Stationary atmospheric responses of geopotential height for SST-0E (A) and SST-180E (B) experiments projected on the barotropic vertical mode ( $Z_{Bt}$ ). Contours are every 2 m, negative contours are dashed, zero contour is omitted and shading is based on magnitude. Plot C: Spatial correlation coefficient (solid line) between  $Z_{Bt}$  responses and the control  $SAM_{Bt}$  (shown in Fig.2-D) and  $\Delta Z_{Bt}$  (dashed line) for the 14 experiments as a function of SSTa forcing longitudes. For each experiment we defined  $\Delta Z_{Bt}$  as the absolute maximum minus minimum of  $Z_{Bt}$  response amplitude, signed with the  $[Z_{Bt}, SAM_{Bt}]$  correlation.  $\Delta Z_{Bt}$  is thus indicative of the meridional direction and amplitude of westerlies response shift (positive: southward, negative: northward). Shaded areas indicate the two very sharp transition regions between the two class of responses.

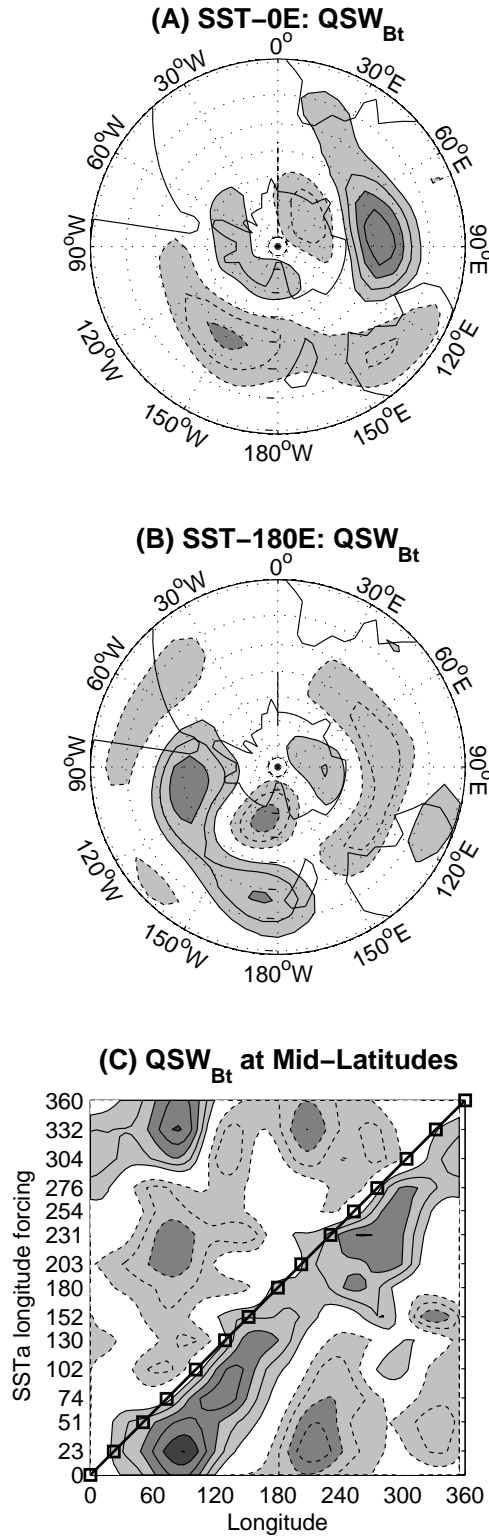


FIG. 6. Plots A-B: Barotropic quasi-stationary wave ( $QSW_{Bt}$ ) responses of geopotential height for SST-0E (A) and SST-180E (B) experiments.  $QSW_{Bt}$  is defined as the zonal asymmetry in the barotropic field  $Z_{Bt}$ , as those shown in Fig.5-A-B. Plot C: 40S-50S mid-latitude average of  $QSW_{Bt}$  as a function of longitude (x-axis) and for all 14 experiments (y-axis). SSTa forcing locations are indicated with black squares on the solid line. For all plots: contours are every  $2m$ , negative contours are dashed, zero contour is omitted and shading is based on magnitude.

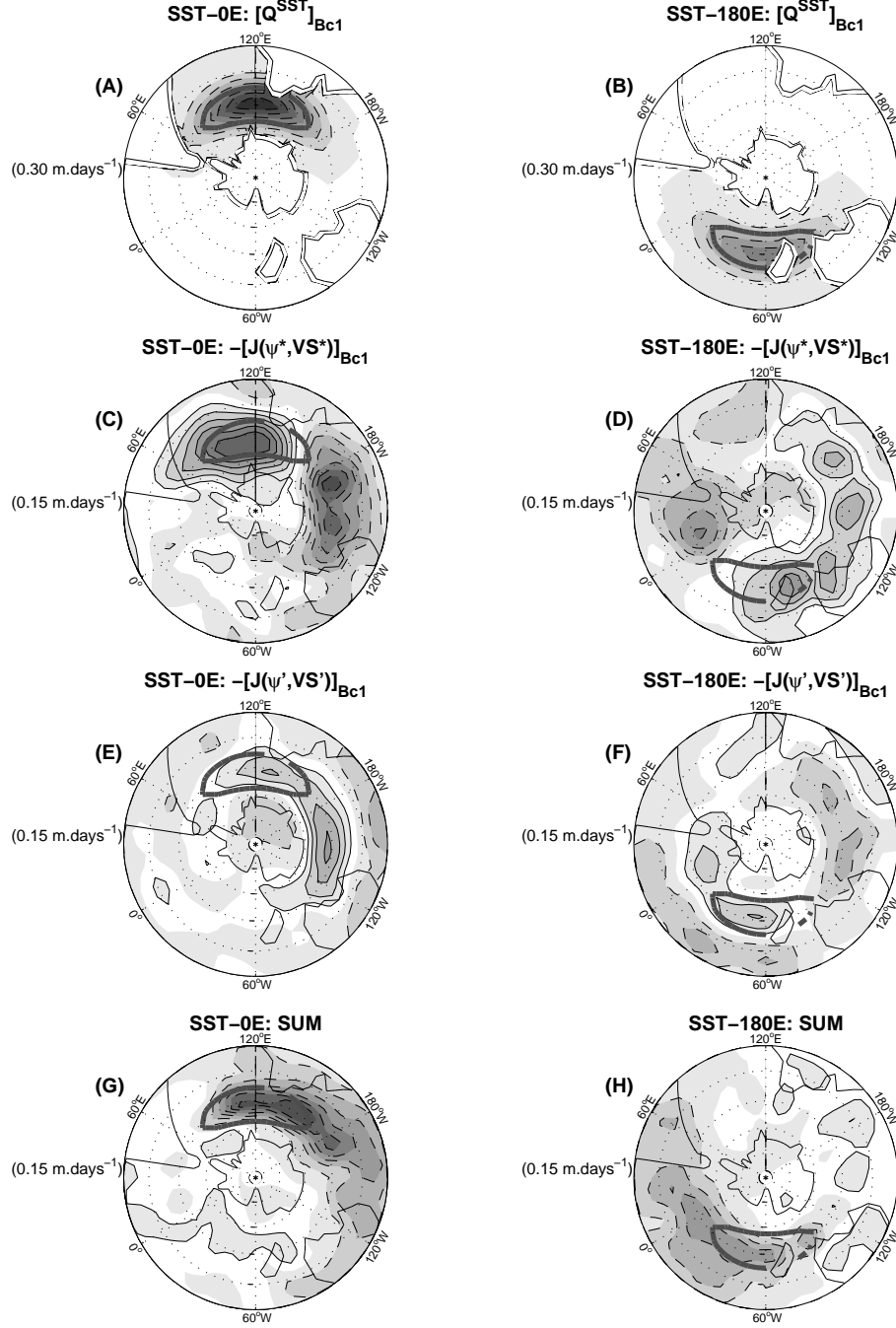


FIG. 7. 1<sup>st</sup> baroclinic mode anomalous PV budget terms, l.h.s. of (15), for experiments SST-0E (left column) and SST-180E (right column). First line (A-B): heat flux term due to the direct forcing of the SSTa:  $[Q^{SST}]_{Bc1}$ . Second line (C-D): PV tendency due to the quasi-stationary vortex stretching flux:  $-[J(\psi^*, VS^*)]_{Bc1}$ . Third line (E-F): PV tendency due to the eddy vortex stretching flux:  $-[J(\psi', VS')]_{Bc1}$ . Fourth line (G-H): Sum of the three terms, responsible for the 1<sup>st</sup> baroclinic mode response shown in Fig.4:A-D. All PV tendencies are plotted as geopotential height tendencies with negative contours dashed, zero contours omitted, with a contour's increment indicated to the left of each plots and a shading based on magnitude. Locations of SST anomalies are indicated by a thick gray line.

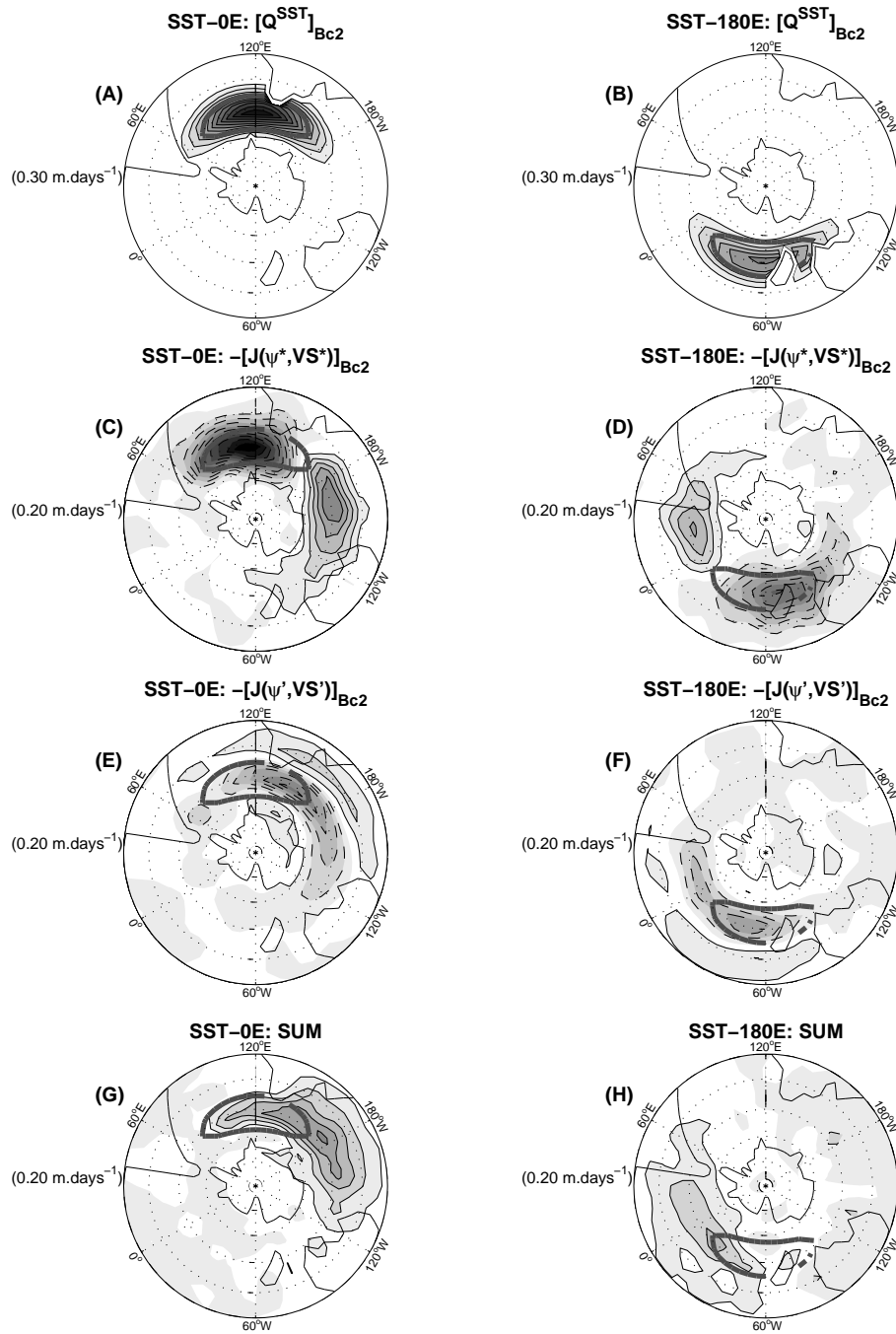


FIG. 8. Same as figure 7 for the 2<sup>nd</sup> baroclinic mode, l.h.s. terms of (15).

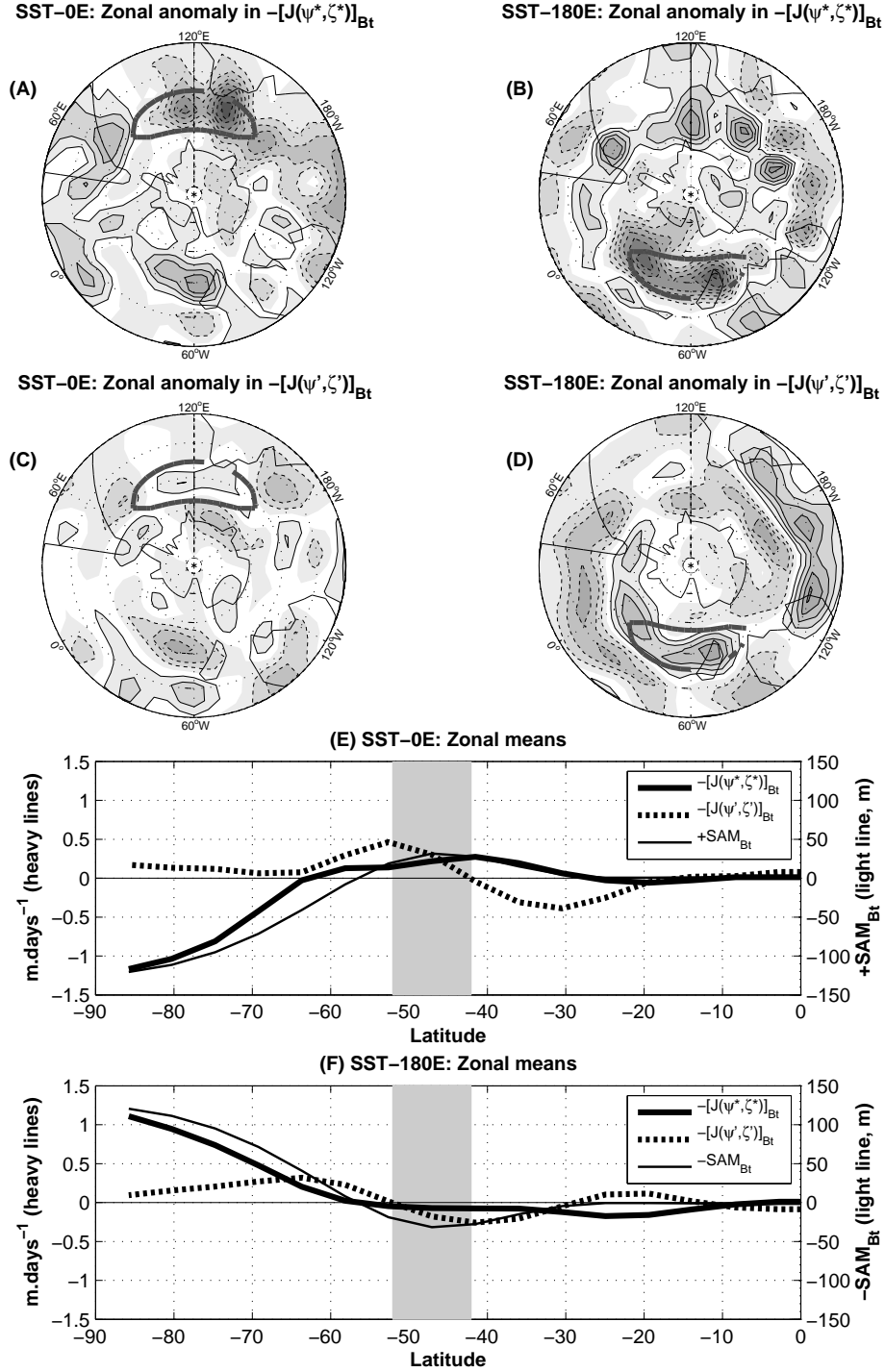


FIG. 9. Plots A to D: Zonal anomalies in the low (first line) and high (second line) frequency relative vorticity fluxes for experiments SST-0E (left) and SST-180E (right) – first and second r.h.s. terms of (13). Contours are every  $0.25 \text{ m days}^{-1}$ , zero contour omitted, negative contours dashed and shading based on magnitude. Locations of SST anomalies are indicated by a thick gray line. Plots E-F: Zonal means of the low (solid) and high (dashed) frequency relative vorticity fluxes for experiments SST-0E (plot E) and SST-180E (plot F). The zonal mean of  $SAM_{Bt}$  in a positive (negative) phase is also plotted in plot E (plot F) as a thin solid line. The SSTa forcing latitude band is highlighted by the gray shaded area.

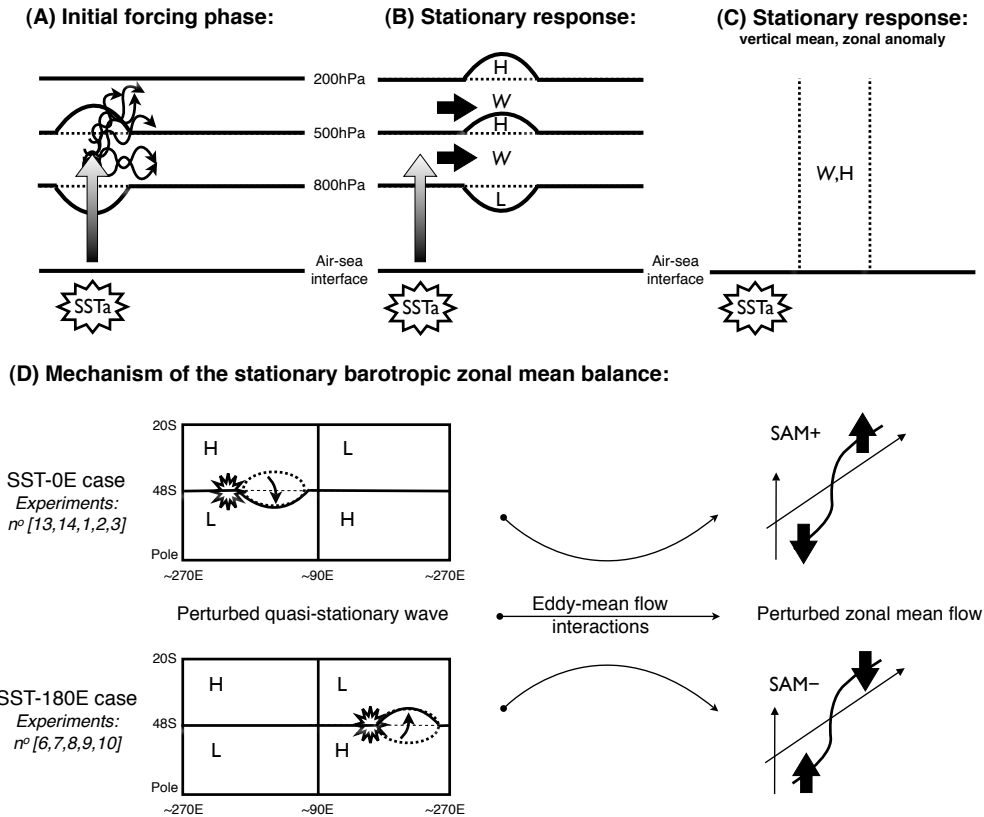


FIG. 10. Plot A: Initial forcing phase of the response with SSTA anomalous heat flux (shaded vertical arrow) inducing a stretching of the lower layer (geopotential heights in solid/dashed black lines) which in turn triggers baroclinic instability (curvy thin arrows). Plot B: Main local balance between heat flux forcing and advection of stretching by the quasi-stationary flow (black plain horizontal arrows). Meridional damping by eddies not shown. "W": warm air and "H/L": high/low pressure anomalies. Plot C: Zonal anomaly of the barotropic response with a barotropic high pressure and warm air anomaly downstream of the SSTA. Plot D: On the left is shown a schematic view of the horizontal  $QSW_{Bt}$  unperturbed field (see Fig.2-C) with succession of highs and lows zonally and meridionally. Superimposed are the SSTA forcing location (black star) and the  $QSW_{Bt}$  high pressure response (dashed ellipse). This perturbation of the climatological quasi-stationary wave pattern interacts with the zonal mean flow through the relative vorticity flux to shift southward/northward the maximum latitude of westerlies (positive and negative phase of the SAM).